CHIN. PHYS. LETT. Vol. 34, No. 10 (2017) 107301

# Spin Caloritronic Transport of (2×1) Reconstructed Zigzag $MoS_2$ Nanoribbons *

Yu-Zhuo Lv(吕钰卓)[1], Peng Zhao(赵朋)[1**], De-Sheng Liu(刘德胜)[2,3]

[1]*School of Physics and Technology, University of Jinan, Jinan 250022*
[2]*School of Physics, Shandong University, Jinan 250100*
[3]*Department of Physics, Jining University, Qufu 273155*

(Received 7 July 2017)

*Using first-principles density functional theory combined with nonequilibrium Green's function method, we investigate the spin caloritronic transport properties of (2×1) reconstructed zigzag $MoS_2$ nanoribbons. These systems can exhibit obvious spin Seebeck effect. Furthermore, by tuning the external magnetic field, a thermal giant magnetoresistance up to $10^4$% can be achieved. These spin caloritronic transport properties are understood in terms of spin-resolved transmission spectra, band structures, and the symmetry analyses of energy bands around the Fermi level.*

*PACS:* 73.23.−b, 85.65.+h, 71.15.Mb DOI: 10.1088/0256-307X/34/10/107301

The dissipating heat becomes a severe problem as the electronic devices shrink toward nanoscale. Excessive dissipating heat not only wastes a large amount of energy, but also deteriorates the performance and reliability of electronic devices. In these respects, spintronics as a promising direction to realize lower energy consumption has drawn much attention.[1,2] On the other hand, thermoelectronics offers a possible way of directly converting dissipating heat into electrical power.[3,4] Recently, spin caloritronics, a research field combining both the advantages of spintronics and thermoelectronics, has attracted extensive interest.[5] Although the concept of spin caloritronics can be traced back to the late 1980s,[6] this field boomed only after the recent experimental discovery of spin Seebeck effect in NiFe, GaMnAs and $LaY_2Fe_5O_{12}$.[7–9] In the spin Seebeck effect, the spin-polarized current can be generated by temperature difference without the need of bias voltage. Moreover, the thermally driven spin-up and spin-down currents flow in opposite directions, which can be further converted to a spin voltage. That is, in this process, the dissipating heat can be directly converted into reusable spin current/voltage.

It is known that molybdenum disulfide ($MoS_2$) one-dimensional (1D) nanostructures such as nanoribbons, nanotubes, wires and rods have recently aroused great interest due to the outstanding physical and chemical properties.[10] In particular, many investigations have been focused on the $MoS_2$ nanoribbons ($MoS_2$NRs). Similar to graphene nanoribbon, there are two typical types of $MoS_2$NRs according to the basic edge configurations: armchair and zigzag $MoS_2$NRs (A$MoS_2$NRs and Z$MoS_2$NRs).[11,12] A$MoS_2$NRs are typical nonmagnetic semiconductors, while Z$MoS_2$NRs are magnetic with sizable magnetic moments on edge atoms.[11,12] However, the existence of dangling bonds along the nanoribbon edge makes these systems unstable. It is well known that edge reconstruction is a common route to remove such dangling bonds.[13–15] Recently, Cui *et al.* revealed (2×1) reconstructed Z$MoS_2$NRs via edge self-passivation mechanism.[16] Very recently, it has been shown that this kind of edge reconstruction mechanism can be used to controllably fabricate transition metal dichalcogenide nanoribbons under nonequlilibrium growth conditions.[17]

It is natural to ask whether these (2×1) reconstructed Z$MoS_2$NRs have the potential in the field of spin caloritronics. To answer this question, in the present work, using the density functional theory (DFT) combined with the nonequilibrium Green's function (NEGF) method, we investigate the spin caloritronic transport properties of these (2×1) reconstructed Z$MoS_2$NRs. Our results show that obvious spin Seebeck effect can be induced in these systems. Moreover, with the help of an external magnetic field, a thermal giant magnetoresistance up to $10^4$% can be achieved.

Figure 1(a) shows the proposed (2×1) reconstructed 6Z$MoS_2$NR-based device, where the prefix 6 indicates the ribbon width according to the conventional notation, i.e., the number of zigzag chains across the ribbon width of original unreconstructed Z$MoS_2$NR. Our test shows that the effect of ribbon width on the following results is very small. The device consists of three parts, namely, the left electrode (LE), the right electrode (RE), and the central scattering region (CSR). The LE/RE is represented by a (2×1) reconstructed 6Z$MoS_2$NR unit cell, while the CSR includes six repeated such unit cells. The vacuum space is set to be 20 Å to avoid the interactions between nanoribbon and its periodic images. Structural relaxation is carried out for the (2×1) reconstructed Z$MoS_2$NR unit cell using the quasi-Newton method until the atomic forces are less than 0.001 eV/Å.

As the magnetization of LE/RE can be controlled by applying external magnetic fields,[18] two distinct magnetic configurations (MCs) are considered: parallel (P) and antiparallel (AP) MCs with magnetic fields at two electrodes pointing in the same ($+y$, $+y$) and

*Supported by the Natural Science Foundation of Shandong Province under Grant No ZR2016AM11.
**Corresponding author. Email: ss_zhaop@ujn.edu.cn

opposite ($+y$, $y$) directions, respectively.

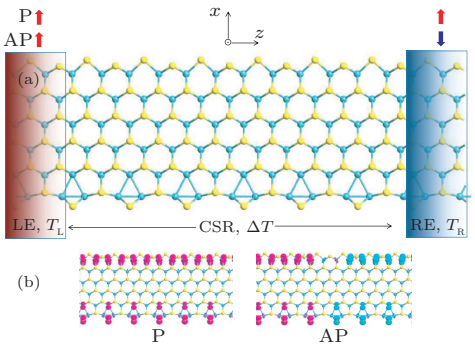


**Fig. 1.** (a) Schematic view of the (2×1) reconstructed 6ZMoS$_2$NR-based spin caloritronic device. Labels LE, RE and CSR denote the left electrode, the right electrode, and the central scattering region, respectively. The thermal spin currents can be generated by the temperature difference ($\Delta T$) between LE ($T_L$) and RE ($T_R$), i.e., $\Delta T = T_L - T_R$. The cyan and yellow balls represent Mo and S atoms, respectively. Labels P and AP represent the magnetic configurations (MCs) of two electrodes. (b) The spin density for the P and AP MCs, where the pink and cyan colors indicate the spin-up and spin-down components, respectively, and the isosurface level is taken as 0.02 |e|/Å$^3$.

The structural relaxation and subsequent spin caloritronic transport properties are both calculated by the DFT+NEGF method, which is implemented in the Atomistix Toolkit (ATK) code.[19–22] The exchange and correlation potential is the Perdew–Burke–Ernzerhof (PBE) functional and is treated using the spin-polarized generalized gradient approximation (SGGA).[23] The core electrons are represented by the Troullier–Martins type norm-conserving pseudopotentials.[24] A double-$\xi$ plus polarization (DZP) basis set is employed for Mo and S atoms. A 150 (350) Ry mesh cutoff and a 1×1×100 (1×1×21) $k$-point grid are used in the transport (relaxation) calculations. The thermally driven spin currents flowing in the device are calculated according to the Landauer–Büttiker formula,[25] $I_\sigma = \frac{e}{h}\int T_\sigma(E)[f_L(E-T_L) - f_R(E-T_R)]dE$, where the spin index $\sigma =$ up (spin-up) or dn (spin-down), $T_\sigma(E)$ is the spin-resolved transmission function for carriers with energy $E$, $T_{L/R}$ and $f_{L/R}$ are the temperature and temperature-dependent Fermi–Dirac distribution function of LE/RE, respectively.

Figure 1(b) plots the spin density ($\Delta\rho = \rho_{up} - \rho_{dn}$) distribution across the CSR for P and AP MCs, where the pink and cyan colors denote the spin-up and spin-down components, respectively. Evidently, the spin density distributes on the edge Mo atoms (edge S atoms and Mo-trimers) at the ribbon top (bottom) edge. Furthermore, the spin density distribution also verifies two MC setups: both the LE and RE are spin-up polarized in the P MC, while the LE/RE is spin-up/spin-down polarized in the AP MC.

We first consider the P MC. Figure 2 shows the calculated thermal spin-resolved currents versus the temperature difference ($\Delta T$) between LE and RE, i.e., $\Delta T = T_L - T_R$, with $T_L$ varying from 300 to 400 K. One can see from Fig. 2 that the spin-up current ($I_{up}$) is positive, while the spin-down current ($I_{dn}$) is negative, i.e., $I_{up}$ and $I_{dn}$ flow in opposite directions. This is an obvious spin Seebeck effect since both $I_{up}$ and $I_{dn}$ are generated by temperature difference rather than by bias voltage.

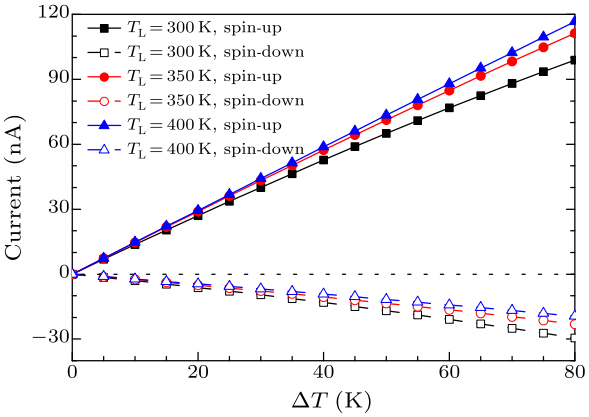


**Fig. 2.** Calculated spin-resolved currents versus $\Delta T$ with $T_L$ varying from 300 to 400 K for the P MC.

According to the Landauer–Büttiker formula, the thermal spin-polarized currents are determined by the combined effects of $T_\sigma$ and $f_{L/R}$. One can know from the Fermi–Dirac distribution that the carrier (hole or electron) concentrations in LE are larger than those in RE since $T_L > T_R$.[26,27] Therefore, both holes and electrons with energy close to the Fermi level $E_F$ diffuse from the hot LE to the cold RE, leading to a positive hole current $I_h$ and a negative electron current $I_e$ in the opposite direction. Moreover, the Fermi–Dirac distribution function is symmetric with respect to $E_F$.[26,27] Then if the transmission is also symmetric about $E_F$, $I_h$ and $I_e$ will cancel out each other, resulting in a zero net thermal current. This indicates that an asymmetric distribution of transmission with respect to $E_F$ is needed to break the electron–hole symmetry and to generate the nonzero thermal current. In the middle panel of Fig. 3, we plot the spin-resolved transmission spectra off the P MC. Clearly, both spin-up and spin-down transmissions are asymmetric about $E_F$. Specifically, a spin-up transmission crosses $E_F$, and the cover area below $E_F$ is larger than that above $E_F$. Hence, $I_h$ is higher than $I_e$, and finally resulting in a positive spin-up $I_h$. In contrast, a spin-down transmission is just above $E_F$ in the energy region [0.015 eV, 0.035 eV], and thus the spin-down transport is dominated by electron carriers, leading to a negative spin-down electron current $I_e$. As a result, the spin Seebeck effect emerges. The origin of these transmissions can be attributed to the band-structures of the (2×1) reconstructed 6ZMoS$_2$NR. The spin-resolved band-structures of LE and RE are presented in the left and right panels of Fig. 3, respectively. Evidently, the bands of LE have the same structures as those of RE, since LE and RE have the same structure and magnetic configuration. To be specific, there are a

spin-down band I and a spin-up band Ⅱ around $E_F$. The spin-up band Ⅱ crosses $E_F$ in the energy region [−0.135 eV, 0.04 eV], while the band I is just above $E_F$ in the energy region [0.015 eV, 0.035 eV]. Thus the overlap of spin-down band I (spin-up band Ⅱ) between LE and RE gives rise to the spin-down (spin-up) transmission around $E_F$.

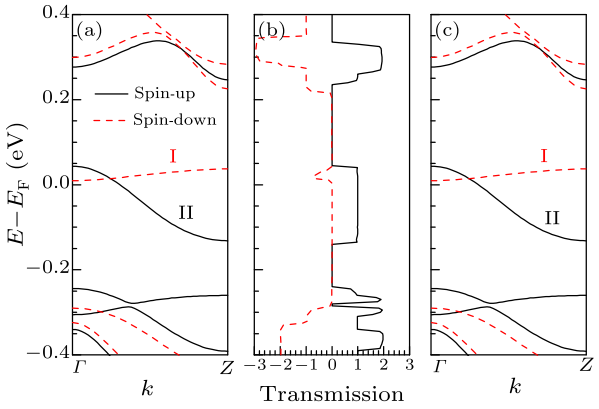


**Fig. 3.** Calculated spin-resolved band-structures of LE (left panel) and RE (right panel), and the spin-resolved transmission spectra (middle panel) of the P MC. In particular, there are a spin-down band I and a spin-up band Ⅱ around $E_F$.

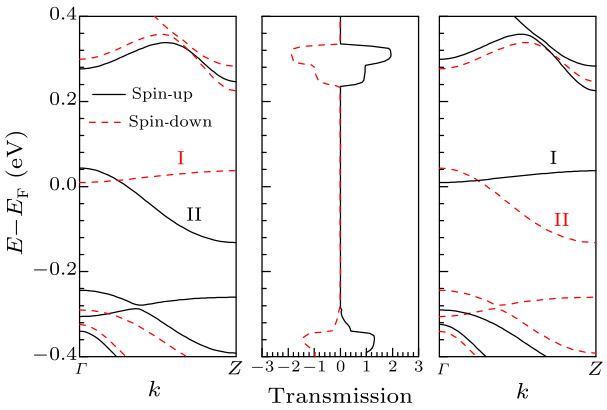


**Fig. 4.** Calculated spin-resolved band-structures of LE (left panel) and RE (right panel), and the spin-resolved transmission spectra (middle panel) of the AP MC.

Now we consider the AP MC. In the middle panel of Fig. 4, we plot the spin-resolved transmission spectra of the AP MC. One can see that the spin-up and spin-down transmission spectra are degenerate, and there is a large transmission gap around $E_F$ from −0.26 eV to 0.24 eV. In the left and right panels of Fig. 4, we plot the band-structures of LE and RE, respectively. Clearly, the spin-up and spin-down band-structures in RE are completely exchanged compared with those in LE when the spin magnetization of RE switches from the P to AP MC. In particular, in the energy region [0.015 eV, 0.035 eV], the spin-down band I (spin-up band Ⅱ) in LE overlaps with the spin-down band Ⅱ (spin-up band I) in RE. However, this overlap cannot contribute any spin-down and spin-up transmission. To clarify this point, in Fig. 5, we plot the Bloch wave function for bands I and Ⅱ at the $\Gamma$ point, respectively. As one can see, the band I is mainly formed by $d_{xy}$ orbitals of the sub-edge Mo atoms and $3p$ orbital of the outmost S atoms at the bottom edge, while the band Ⅱ is mainly dominated by $d_y^2$ orbitals of the sub-edge Mo atoms at the top edge. Moreover, the symmetry of two bands is completely opposite, namely, the bands I and Ⅱ have odd and even parities under the $xz$ midplane mirror operation, respectively, leading to the transmission be forbidden from LE to RE,[28,29] and form the transmission gap in the energy region [0.015 eV, 0.035 eV] in the AP MC.

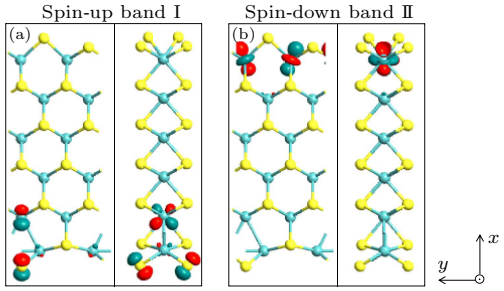


**Fig. 5.** Calculated Bloch wave function for bands I (a) and Ⅱ (b) at the $\Gamma$ point. The isosurface level is taken as 0.2/(Å$^3$·eV).

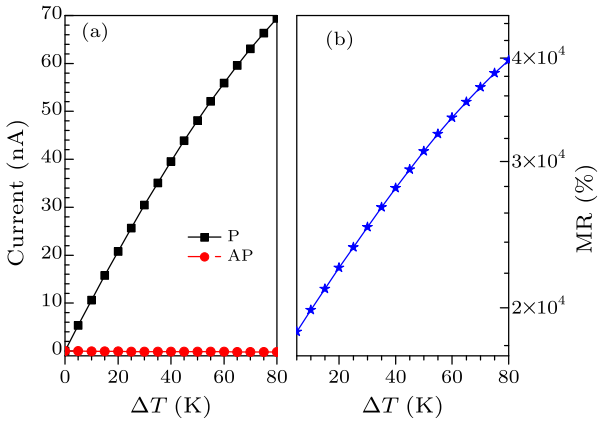


**Fig. 6.** (a) Calculated total thermal current for the P and AP MCs with $T_L = 300$ K at different $\Delta T$. (b) The calculated MR versus $\Delta T$ with $T_L = 300$ K.

Since there is a large transmission gap around $E_F$, both the spin-up and spin-down transmissions are almost bilaterally symmetric in the vicinity of $E_F$. Then one can expect that both the thermally driven spin-up and spin-down currents are close to zero. In Fig. 6(a), we present the total thermal current (sum of $I_{up}$ and $I_{dn}$) for the P and AP MCs with $T_L = 300$ K at different $\Delta T$. It is clear that the total thermal current in the P MC is much larger than that in the AP MC, and actually, the total thermal current in the AP MC is almost completely blocked. As a result, a thermal giant magnetoresistance (GMR) effect can be realized when the spin magnetization of RE switches between the P and AP MCs. The thermal GMR effect can be quantitatively evaluated by the magnetoresistance ratio (MR), which is defined as

MR $= [(|I_{\rm P}|-|I_{\rm AP}|)/|I_{\rm AP}|]\times 100\%$, where $I_{\rm P}$ and $I_{\rm AP}$ are the total thermal currents in the P and AP MCs, respectively. Figure 6(b) plots the MR versus $\Delta T$. As one can see, the MR is higher than $10^4\%$.

In conclusion, we have investigated the spin caloritronic transport properties of (2×1) reconstructed $ZMoS_2$NRs using the first-principles DFT+NEGF method. Our results show that obvious spin Seebeck effect can be observed in these systems. The reason can be attributed to the asymmetry of the spin-resolved transmission spectra about $E_{\rm F}$, which breaks the electron–hole symmetry. Moreover, by tuning the external magnetic field, a thermal giant MR up to $10^4\%$ can be achieved. These results demonstrate that (2×1) reconstructed $ZMoS_2$NRs are promising candidates for spin caloritronic devices.

## References


[1] Wolf S, Awschalom D, Buhrman R, Daughton J, von Molnar S, Roukes M, Chtchelkanova A and Treger D 2001 *Science* **294** 1488
[2] Fert A 2008 *Rev. Mod. Phys.* **80** 1517
[3] Zebarjadi M, Esfarjani K, Dresselhaus M S, Ren Z F and Chen G 2012 *Energy Environ. Sci.* **5** 5147
[4] Poehler T O and Katz H E 2012 *Energy Environ. Sci.* **5** 8110
[5] Bauer G E W, Saitoh E and van Wees B J 2012 *Nat. Mater.* **11** 391
[6] Bauer G E W, MacDonald A H and Maekawa S 2010 *Solid State Commun.* **150** 459
[7] Uchida K, Takahashi S, Harii K, Ieda J, Koshibae W, Ando K, Maekawa S and Saitoh E 2008 *Nature* **455** 778
[8] Jaworski C M, Yang J, Mack S, Awschalom D D, Heremans J P and Myers R C 2010 *Nat. Mater.* **9** 898
[9] Uchida K, Xiao J, Adachi H, Ohe J, Takahashi S, Ieda J, Ota T, Kajiwara Y, Umezawa H, Kawai H, Bauer G E W, Maekawa S and Saitoh E 2010 *Nat. Mater.* **9** 894
[10] Xia Y, Yang P, Sun Y, Wu Y, Mayers B, Gates B, Yin Y, Kim F and Yan H 2003 *Adv. Mater.* **15** 353
[11] Li Y, Zhou Z, Zhang S and Chen Z 2008 *J. Am. Chem. Soc.* **130** 16739
[12] Botello-Méndez A R, López-Urías F, Terrones M and Terrones H 2009 *Nanotechnology* **20** 325703
[13] Lauritsen J V, Kibsgaard J, Helveg S, Topøe H, Clausen B S, Lægsgaard E and Besenbacher F 2007 *Nat. Nanotechnol.* **2** 53
[14] Hansen L P, Ramasse Q M, Kisielowski C, Brorson M, Johnson E, Topsøe H and Helveg S 2011 *Angew. Chem. Int. Ed.* **50** 10153
[15] Zhou W, Zou X L, Najmaei S, Liu Z, Shi Y M, Kong J, Lou J, Ajayan P M, Yakobson B I and Idrobo J C 2013 *Nano Lett.* **13** 2615
[16] Cui P, Choi J H, Chen W, Zeng J, Shih C K, Li Z and Zhang Z 2017 *Nano Lett.* **17** 1097
[17] Chen Y, Cui P, Ren X, Zhang C, Jin C, Zhang Z and Shih C K 2017 *Nat. Commun.* **8** 15135
[18] Son Y W, Cohen M L and Louie S G 2006 *Nature* **444** 347
[19] Taylor J, Guo H and Wang J 2001 *Phys. Rev.* B **63** 121104(R)
[20] Taylor J, Guo H and Wang J 2001 *Phys. Rev.* B **63** 245407(R)
[21] Brandbyge M, Mozos J L, Ordejón P, Taylor J and Stokbro K 2002 *Phys. Rev.* B **65** 165401
[22] Soler J M, Artacho E, Gale J D, García A, Junquera J, Ordejón P and Sánchez-Portal D 2002 *J. Phys.: Condens. Matter* **14** 2745
[23] Perdew J P, Burke K and Ernzerhof M 1996 *Phys. Rev. Lett.* **77** 3865
[24] Troullier N and Martins J 1991 *Phys. Rev.* B **43** 1993
[25] Büttiker M, Imry Y, Landauer R and Pinhas S 1985 *Phys. Rev.* B **31** 6207
[26] Wu Q H, Zhao P, Su Y, Liu D S and Chen G 2015 *RSC Adv.* **5** 20699
[27] Wu Q H, Zhao P and Liu D S 2016 *Chin. Phys. Lett.* **33** 037303
[28] Li Z Y, Qian Y, Wu J, Gu B L and Duan W H 2008 *Phys. Rev. Lett.* **100** 206802
[29] Wang Z F, Li Q X, Shi Q W, Wang X P, Yang J L, Hou J G and Chen J 2008 *Appl. Phys. Lett.* **92** 133114